

Enhancing Object Coherence in Layout-to-Image Synthesis

Yibin Wang^{1, 2*}, Weizhong Zhang^{1*}, Jianwei Zheng², Cheng Jin^{1†}

¹College of Computer Science and Technology, Fudan University

²College of Computer Science and Technology, Zhejiang University of Technology

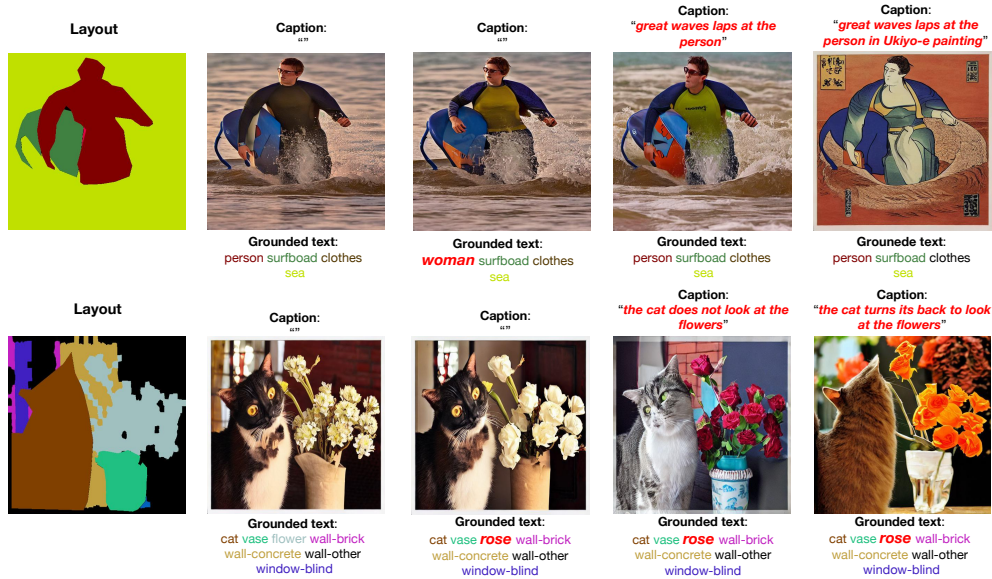


Figure 1. Displayed are the LIS outcomes generated using our model. Each instance comprises three inputs: a semantic mask layout, grounded text, and caption. To exemplify our model’s capabilities comprehensively, we present four exemplar outcomes for each layout, showcasing the versatility of our approach by using edited texts and captions.

Abstract

Layout-to-image synthesis is an emerging technique in conditional image generation. It aims to generate complex scenes, where users require fine control over the layout of the objects in a scene. However, it remains challenging to control the object coherence, including semantic coherence (e.g., the cat looks at the flowers or not) and physical coherence (e.g., the hand and the racket should not be misaligned). In this paper, we propose a novel diffusion model with effective global semantic fusion (GSF) and self-similarity feature enhancement modules to guide the object coherence for this task. For semantic coherence, we argue that the image caption contains rich information for defining the semantic relationship within the objects in the images. Instead of simply employing cross-attention between captions and generated images, which addresses the highly relevant layout restriction and semantic coherence separately and thus

leads to unsatisfying results shown in our experiments, we develop GSF to fuse the supervision from the layout restriction and semantic coherence requirement and exploit it to guide the image synthesis process. Moreover, to improve the physical coherence, we develop a Self-similarity Coherence Attention (SCA) module to explicitly integrate local contextual physical coherence into each pixel’s generation process. Specifically, we adopt a self-similarity map to encode the coherence restrictions and employ it to extract coherent features from text embedding. Through visualization of our self-similarity map, we explore the essence of SCA, revealing that its effectiveness is not only in capturing reliable physical coherence patterns but also in enhancing complex texture generation. Extensive experiments demonstrate the superiority of our proposed method in both image generation quality and controllability. Our model outperforms the previous SOTA methods on FID and DS by relatively 0.9, 3.3% on

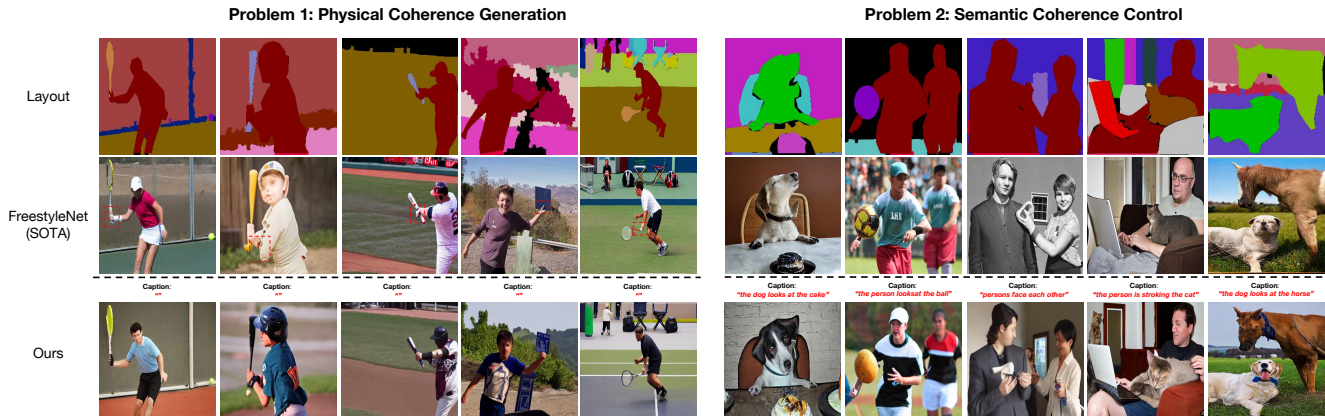


Figure 2. The prevailing challenges of physical coherence and semantic coherence. We omit the grounded text for simplicity and highlight the physical coherence problem using the red outline.

COCO-stuff, and 1.1 3.2% on ADE20K.

1. Introduction

Layout-to-image synthesis (LIS) enables the generation of images portraying distinct subjects in diverse scenes. In this task, various types of layouts are employed, including bboxes+classes [8, 45], semantic masks+classes [25, 33, 42], skeletons [17, 21], and more. In this work, we focus on the type of semantic masks. Earlier studies on mask-based LIS [19, 25, 33, 39, 41] employ generative adversarial networks (GANs). However, these GAN-based approaches often face challenges related to unstable convergence [2] and mode collapse [26]. Therefore, recent studies [38, 42] utilize some large-scale pre-trained text-to-image diffusion models like stable diffusion [28] to achieve LIS. These pre-trained models exhibit a generative prior with a broad spectrum of semantics, enabling the synthesis of diverse unseen objects.

However, these methods [19, 25, 32, 33, 41, 42] still encounter critical challenges concerning object coherence, including semantic coherence (e.g., the cat looks at the flowers or not), and physical coherence (e.g., the hand and the racket should not be misaligned). Taking the recent method, FreestyleNet [42], as an example, which introduced Rectified Cross Attention (RCA) to generate unseen objects from given layouts, it fails to freely control the objects’ semantic interactions. Besides, RCA’s region-specific token influence neglects implicit physical coherence restrictions between neighboring objects, resulting in unsatisfied image synthesis. The qualitative examples presented in Fig. 2 serve as compelling illustrations of these problems. We posit that the suboptimal physical generation stems from their inability to capture potential physical coherent restrictions in the layout. Moreover, the failure to control semantic coherence can be attributed to their neglect to incorporate semantic interaction

requirements.

In this paper, we propose a novel diffusion model dubbed EOCNet, equipped with our Global Semantic Fusion (GSF) and Self-similarity Feature Enhancement (SFE) modules. These components are designed to address semantic coherence and physical coherence problems, respectively, which will be elaborated as follows.

First, GSF is tailored to excavate the capability for semantic coherence control by integrating semantic coherence requirements into the image generation process. These requirements are defined through our innovatively introduced caption input. It’s crucial to note that our caption differs from certain text-to-image studies [15, 28, 29] that use captions to specify objects’ class and position (e.g., ”a bag on the desk, next to a vase”), as these are already defined by our grounded text and layout. Given that the relative positions of objects in the layout inherently restrict their semantic coherence interactions in this task, GSF avoids naive methods (e.g., direct cross-attention [37] between caption embedding and images [28]) that separately address layout restrictions and semantic coherence requirements. Instead, GSF effectively merges semantic interaction requirements with spatial restrictions. Specifically, in each time step, GSF first integrates supervision information from the layout map and caption embedding through transformer blocks [37]. Subsequently, it integrates these amalgamated restriction features into the generated image, providing a comprehensive understanding of both semantic and spatial constraints. This cohesive process effectively guides the image synthesis.

On the other hand, SFE leverages the effective synergy between RCA and our Self-similarity Coherence Attention (SCA) to enhance the physical coherence generation. To be precise, it extends the superiority of RCA [42] and remedies its drawback through our ingeniously designed SCA. To explicitly integrate inherent physical coherence restrictions into each pixel’s generation process, SCA revolutionizes the way

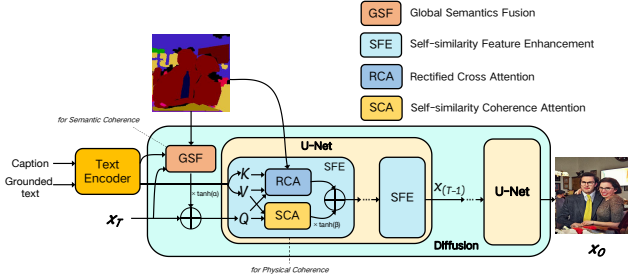


Figure 3. An overview of our EOCNet. We propose Global Semantics Fusion and Self-similarity Feature Enhancement (SFE) modules to address the semantic coherence and physical coherence problems. SFE takes the cross-attention’s place in the U-net. It leverages the effective synergy between Rectified Cross Attention and our Self-similarity Coherence Attention.

each pixel interacts with its neighboring features, effectively capturing local contextual physical coherence relations. It encodes these relations into vectors, generating similarity maps that encapsulate rich coherence relationships between each pixel and its contextual features. These maps are then utilized to extract features with potential physical coherence restrictions from text embeddings. This process enhances the generator’s ability to comprehend intricate physical coherence relationships in the layout, contributing to optimal physical coherence generation. To form a synergy between RCA and SCA, their outputs are fused, allowing the model to leverage SCA’s fine-grained understanding of local context while retaining RCA’s proficiency in generating previously unseen objects [42].

We evaluate our model on COCO-Stuff [4] and ADE20K [46], and our model outperforms the previous SOTA methods on FID and DS by relatively 0.9, 3.3% on COCO-stuff, and 1.1, 3.2% on ADE20K. The visualized self-similarity maps in SCA validate its innate proficiency in discerning dependable physical coherence patterns. Notably, it also underscores SCA’s surprising efficacy in enhancing the generation of complex textures. This multifaceted superiority of SCA propels the model’s capability to yield more high-fidelity images.

Our main contributions are threefold.

- We address the coherence problems in LIS. Specifically, we excavate the capability for semantic coherence control and improve the physical coherence generation, achieving greater controllability and higher generation quality.
- By exploring the essence of our SCA, we reveal its effectiveness not only in capturing reliable physical coherence patterns but also in enhancing complex texture generation.
- Our model outperforms the previous SOTA methods on FID and DS by relatively 0.9, 3.3% on COCO-stuff and 1.1, 3.2% on ADE20K

2. Related Work

2.1. Semantic Layout Image Synthesis

This task aims to generate multiple objects in diverse scenes using given semantic layouts [1, 12, 19, 22, 25, 31, 33–35, 39–41, 47–49]. Existing approaches have been explored in the field of semantic image synthesis. For instance, Pix2Pix [12] employs an encoder-decoder generator with a PatchGAN discriminator. Pix2PixHD [39] builds on Pix2Pix by introducing coarse-to-fine and multi-scale network architectures to handle high-resolution image synthesis. SPADE [25] modulates the activations in normalization layers using affine parameters predicted from input semantic maps. On the other hand, CC-FPSE [19] and SC-GAN [41] adopt a different approach by learning to generate convolutional kernels and semantic vectors from the semantic maps to condition the image generation process. Additionally, OASIS [33] introduces a segmentation-based discriminator to improve image alignment with the input label maps. Despite their impressive performance, these methods suffer from challenges such as unstable convergence and model collapse, mainly due to their reliance on GANs. These issues can result in artifacts and a lack of coherence in the generated images, limiting their overall quality. Recognizing GANs’ inherent limitations, PITI [38] pioneeringly adopts a pre-trained diffusion model to enhance image-to-image translation. Following this, FreestyleNet [42] introduces a freestyle LIS framework, emphasizing controllability. This framework empowers the generation of semantics beyond the confines of pre-defined semantic categories present in the training dataset. However, they are still facing critical challenges concerning object coherence. In this paper, we present our framework to tackle both semantic and physical coherence in the LIS task. Our primary goal is to introduce a novel method that achieves superior generation quality and enhanced controllability compared to the mentioned approaches.

2.2. Diffusion Model

Diffusion models [3, 11, 23, 28, 43] are emerging as promising generative models, setting new benchmarks in image generation across various domains [5, 7, 36, 43], including class-conditional [6, 44], text-to-image [15, 28, 29], and image-to-image translation tasks [13, 14, 20, 24, 30]. Notably, ADM-G [6] explores the classifier guidance, using the classifier’s gradient on noisy images during sampling. Further, Ho et al. [10] introduce a classifier-free approach by interpolating between predictions of a diffusion model with and without conditional input. For efficient training and sampling, LDM compresses images to a smaller resolution and employs denoising training in the latent space.

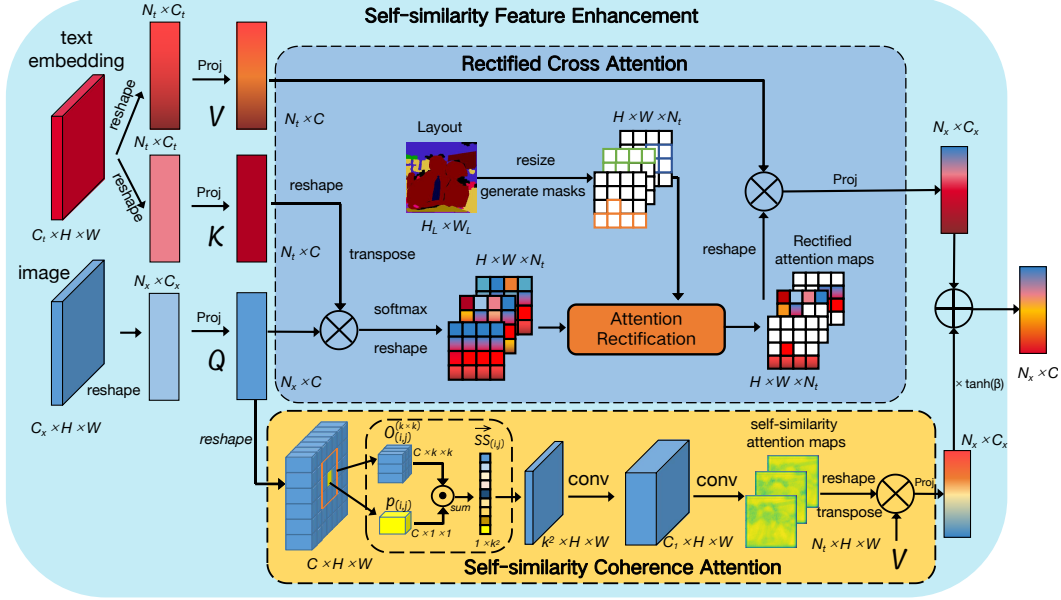


Figure 4. The pipeline of our Self-similarity Feature Enhancement module.

3. Method

In this section, we will begin by providing an overview and the training pipeline of our method. Following that, we will provide a detailed explanation of the Global Semantics Fusion (GSF) module. Subsequently, we will delve into the intricacies of the Self-similarity Feature Enhancement (SFE) module, shedding light on its fundamental role in fostering a synergistic interplay between Self-similarity Coherence Attention (SCA) and Rectified Cross Attention (RCA).

3.1. Overview

In this work, we aim to tackle both semantic coherence and physical coherence in the LIS task. As illustrated in Fig. 3, our approach incorporates the GSF to integrate semantic coherence requirements into the synthesis process and employs SFE to enhance the generation of physical coherence. Given the initial noise image z_T perturbed by Gaussian noise ε , grounded text, caption, and semantic mask, we first stack all concepts from the grounded text. Then we feed the stacked concepts and the caption into the text encoder CLIP [27], outputting text embedding $y_g \in \mathbb{R}^{C_t \times N_t}$ and caption embedding $y_e \in \mathbb{R}^{C_t \times N_t}$, where C_t and N_t denote the amount of channels and tokens respectively. After that, we resize the single-channel semantic layout to align with the spatial dimensions of the noise images $z_T \in \mathbb{R}^{C \times H \times W}$ using interpolation, yielding the layout embedding $S \in \mathbb{R}^{1 \times H \times W}$, where H and W denote the height and width. Based on these, our approach synthesizes the image z_0 over T time steps in a progressive and evolving manner.

3.2. Training Process

In each time step t , EOCNet first fuses supervision information from the layout embedding S and caption embedding y_e through GSF. Then, these amalgamated supervision features are infused into the noise image x_t to steer the image synthesis effectively. After that, the constricted image x'_t will be input to the U-Net ε_θ whose cross-attention layer is replaced with our SFE. Illustrated in Fig. 4, SFE facilitates a dynamic interplay between RCA and SCA. Precisely, RCA restricts each token embedding to influence only its corresponding area, while SCA encodes local potential coherence relations of each pixel into self-similarity maps, thereby enhancing the generation of physical coherence. Ultimately, the output features of SCA and RCA are amalgamated, yielding the final output of SFE.

The objective loss for our fine-tuning is formulated as follows:

$$L(\theta) = \mathbb{E}_{z_t, S, y_g, y_e, \varepsilon \sim \mathcal{N}(0,1), t} \left[\|\varepsilon - \varepsilon_\theta(z_t, t, S, y_g, y_e)\|_2^2 \right].$$

3.3. Global Semantics Fusion

GSF is tailored to achieve semantic coherence control by simultaneously integrating semantic coherence requirements and layout restriction into the image generation process. Specifically, It first employs L sequential layers of classical self- and cross-attention blocks [37] to effectively integrate the supervision information from layout embedding $S \in \mathbb{R}^{1 \times H \times W}$ and caption embedding $y_e \in \mathbb{R}^{C_t \times N_t}$. First, it concatenate z_t and S , followed by employing a linear mapping to obtain $S' \in \mathbb{R}^{C \times H \times W}$. Then, the integration process

within layer $l \in [1, L]$ can be formulated as follows.

$$F_l = \text{SelfAtt}(\mathbf{O}_{l-1}, \mathbf{O}_{l-1}, \mathbf{O}_{l-1}) + \mathbf{O}_{l-1}, \quad (1)$$

$$F'_l = \text{CrossAtt}(F_l, \mathbf{y}_e, \mathbf{y}_e) + F_l, \quad (2)$$

$$\mathbf{O}_l = F'_l \mathbf{W}_l, \quad (3)$$

where $\mathbf{O}_l, F_l, F'_l \in \mathbb{R}^{C \times H \times W}$, $\mathbf{O}_0 = \mathbf{S}'$ and \mathbf{W}_l representing the parameters of the feedforward layer. \mathbf{O}_L is the output of GSF.

To infuse amalgamated supervision features into the image, a straightforward approach is to directly incorporate \mathbf{O}_L into the image features \mathbf{z}_t [45]. This process can be defined as

$$\mathbf{z}'_t = \mathbf{z}_t + \tanh(\alpha) * \mathbf{O}_L, \quad (4)$$

where α represents a learnable parameter initialized with a value of 0.

3.4. Self-similarity Feature Enhancement

We propose SFE that fosters a dynamic interplay between RCA and SCA to substitute the cross-attention layer within the U-Net. In this section, we will first introduce RCA's effectiveness in restricting each token's influence over pixels within the specific region. Then, we will delve into the details of SCA on guiding each pixel to engage with its neighboring features. Finally, the fusion mode of the output features from SCA and RCA is elaborated.

3.4.1 Rectified Cross Attention

We utilize the RCA elaborated in [42] to ensure that each object (defined by grounded text) is generated within the region defined by the layout. It compels each text token to influence the designated region by rectifying the computed attention maps. Specifically, given the image feature maps and text embedding \mathbf{y}_g , SFE computes image queries $\mathbf{Q} \in \mathbb{R}^{N_x \times C}$, text keys \mathbf{K} , and text values $\mathbf{V} \in \mathbb{R}^{N_t \times C}$ through three separate projection layers, where N_x represents the number of flattened pixels. The rectified process can be denoted as

$$\mathbf{I}_{RCA} = \text{RCA}(\mathbf{Q}, \mathbf{K}, \mathbf{V}). \quad (5)$$

Here, $\mathbf{I}_{RCA} \in \mathbb{R}^{N_x \times C_x}$ is the output image feature. Detailed operations can be found in the original paper [42].

3.4.2 Self-similarity Coherence Attention

RCA's region-specific token influence neglects implicit physical coherence restrictions between neighboring objects, thus we propose SCA to explicitly integrate inherent physical coherence restriction into each pixel's generation process. Specifically, SCA calculates the similarity between each

pixel and its spatial adjacent feature within a defined local neighborhood region. As illustrated in Fig. 4, it first reshapes the given image query to obtain $\mathbf{Q}_r \in \mathbb{R}^{C \times H \times W}$. Then, we apply zero-padding of size $(k-1)/2$ (assuming k is odd) to \mathbf{Q}_r , resulting in the padded feature map $\tilde{\mathbf{Q}} \in \mathbb{R}^{C \times (H+k-1) \times (W+k-1)}$. This padding operation ensures that border pixels on the feature map are included in local self-similarity computation. After that, for any position x_{ij} in the feature maps $\tilde{\mathbf{Q}}$, where $x_{ij} \in \mathbb{R}^{C \times 1 \times 1}$, we construct a local neighbor region of spatial size (k, k) centered at x_{ij} , denoted as $\mathbf{O}_{ij}^{k \times k} \in \mathbb{R}^{C \times k \times k}$. Next, we compute the dot product between x_{ij} and each neighboring position within the local region $\mathbf{O}_{ij}^{k \times k}$ and then sum the resulting vector across the channel dimension. This process yields the self-similarity vector $\vec{\mathbf{s}}_{i,j} \in \mathbb{R}^{k^2 \times 1}$. Then, all pixel's vectors constitute the self-similarity features map $\mathbf{SS} \in \mathbb{R}^{k^2 \times H \times W}$. The process of generating the self-similarity feature map can be formulated as follows:

$$t = (k-1)/2, \quad (6)$$

$$\vec{\mathbf{s}}_{i,j} = [\tilde{\mathbf{x}}_{i-t,j-t}^T \cdot \mathbf{x}_{i,j}, \dots, \tilde{\mathbf{x}}_{i+t,j+t}^T \cdot \mathbf{x}_{i,j}], \quad (7)$$

$$\mathbf{SS} = \vec{\mathbf{s}}_{1,1}, \dots, \vec{\mathbf{s}}_{H,W}. \quad (8)$$

Here, $\mathbf{x}_{i,j}$ and $\tilde{\mathbf{x}}_{i,j}$ represent the spatial positions (i, j) within the feature map \mathbf{Q} and the padded feature map $\tilde{\mathbf{Q}}$, respectively. The hyperparameter k denotes the length of the local neighbor region. $\vec{\mathbf{s}}_{i,j}$ signifies the self-similarity vector at spatial position (i, j) within the feature map, and the self-similarity feature map $\mathbf{SS} \in \mathbb{R}^{k^2 \times H \times W}$ is an aggregation of these self-similarity vectors $\vec{\mathbf{s}}$.

Note that the local region size k restricts the interaction scope of each pixel. This limitation results in the self-similarity feature map failing to encompass comprehensive contextual physical coherence information. To address this limitation, we employ convolution layers to expand the context and further capture intricate self-similarity patterns:

$$\mathbf{M} = \text{ReLU}(\text{Conv}_2(\text{ReLU}(\text{Conv}_1(\mathbf{SS})))), \quad (9)$$

where $\mathbf{M} \in \mathbb{R}^{N_t \times H \times W}$ is the generated self-similarity maps. Its empirical validations are presented in Sec. 4.4.

Subsequently, we reshape and transpose the self-similarity maps and obtain $\mathbf{M} \in \mathbb{R}^{N_x \times N_t}$. Finally, the output image feature $\mathbf{I}_{SCA} \in \mathbb{R}^{N_x \times C_x}$ can be calculated by:

$$\mathbf{I}_{SCA} = \text{Proj}(\text{Softmax}(\mathbf{M})\mathbf{V}), \quad (10)$$

where Proj denotes the projection.

3.4.3 Fusing Feature Maps

To foster a dynamic interplay between RCA and SCA, SFE amalgamates the output maps \mathbf{I}_{RCA} and \mathbf{I}_{SCA} from them

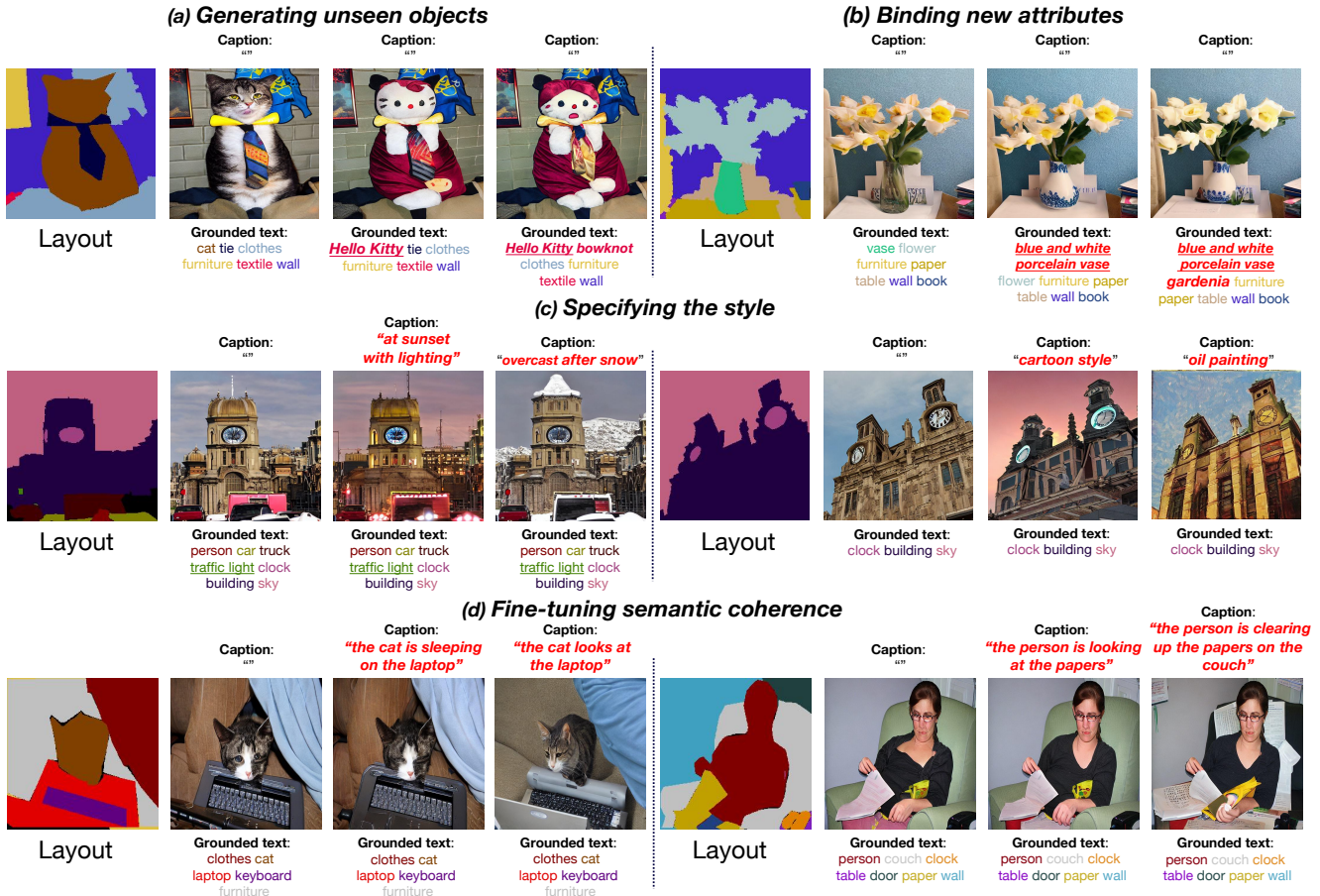


Figure 5. Exemplar results and demonstrated capabilities of our EOCNet. Zooming in for better visibility and detail.

using a trainable parameter β , formulated as

$$I_{SFE} = I_{RCA} + \tanh(\beta) * I_{SCA}. \quad (11)$$

This fusion empowers the model to leverage SCA’s fine-grained understanding of potential local contextual coherence restrictions, thereby enhancing physical coherence generation. Simultaneously, it retains RCA’s expertise in generating previously unseen objects.

4. Experiments

4.1. Implementation details

Datasets. We employ two datasets, COCO-Stuff [4] and ADE20K [46]. COCO-Stuff comprises 118,287 training and 5,000 validation images, annotated with 182 semantic classes. ADE20K contains 20,210 training and 2,000 validation images, encompassing 150 semantic classes.

Training figures. We adopt the origin training set of Stable Diffusion [28] unless specific noted and fine-tune our model based on the *stable-diffusion-v1.4*. The base learning rate is 10^{-6} . We use the BLIP-2 model [16] *blip2-opt-6.7b-coco* to generate captions for all images in COCO-Stuff and

train our model on COCO-Stuff/ADE20K takes approximately 4/1 days on 4 NVIDIA A100 GPUs. We use 50 PLMS [18] steps with a scale of 2 for classifier-free guidance [10].

Evaluation metrics. We evaluate all the baselines using the pre-trained models obtained from their source codes. We use mean Intersection over-Union (mIoU) to measure the segmentation accuracy and Fréchet Inception Distance (FID) [9] to measure the distribution distance between the synthesized results and real images. For diversity comparison. We assess diversity using Diversity Score (DS) akin to [33].

Baselines. Following [42], we compare our method against the state-of-the-art LIS baselines including Pix2PixHD [39], SPADE [25], CC-FPSE [19], OASIS [33], SC-GAN [41], PITI [38] and FreestyleNet [42].

4.2. Qualitative Evaluation

Superiority compared with SOTA. Current SOTA LIS diffusion models [42] utilize semantic masks to determine object positioning and employ textual inputs to control object classes. Our model inherits these functionalities while intro-



Figure 6. Qualitative comparative results against state-of-the-art LIS methods on COCO-Stuff (upper 2 rows) and ADE20K (lower 2 rows). The captions of all the cases are set to empty for our model and we omit the grounded text for simplicity.

ducing novel enhancements to achieve greater controllability and higher generation quality. Specifically, by introducing the caption as input and utilizing our GSF to integrate semantic scene or overall style requirements into the generation process, our model gains the power to finely tune semantic coherence in the resulting image and control its style. On the other hand, we also propose SFE that leverages SCA’s fine-grained understanding of local contextual coherence relations to improve physical coherence generation.

Qualitative Results Evaluation. Through encapsulating objects’ classes within the input text and specifying semantic coherence requirements in the caption, our model effectively synthesizes compelling images. We highlight four distinct capabilities of our proposed model in Fig. 5, placing particular emphasis on the caption’s role in style specification (2nd row) and semantic coherence tuning (3rd row). The synergistic results of all capabilities are demonstrated in Fig. 1. The effectiveness of our model in addressing object coherence challenges is shown in Fig. 2. These results demonstrate that our model faithfully generates images portraying the novel objects and semantic scenes described in the input text and caption respectively. It’s important to note again that our caption can not only specify the image style but also adjust the semantic coherence between objects. For instance, the 3rd row of Fig. 5, demonstrates how the cat interacts with the laptop as dictated by the caption.

4.3. Comparison with LIS Baselines

Quantitative results. As illustrated in Tab. 1, our proposed EOCNet excels across the board, surpassing all competitors in both FID and DS metrics. This underscores the remark-

able visual quality and diversity of the images generated through our approach. Notably, the recent FreestyleNet also showcases commendable generation quality. However, its reliance solely on RCA to constrain text token influence within designated regions leads to the omission of potential physically coherent relationships between objects in the layout. As a consequence, its realism and naturalness in terms of physical coherence generation are compromised. Our model yields comparatively lower mIoU scores in contrast to certain other LIS methods. This observation is in line with the argument presented in [42], where it is asserted that mIoU might not be an entirely suitable metric for evaluating models involving RCA. This limitation arises from the potential generation of more generalized semantics driven by pre-trained knowledge (e.g., the building in the 3rd row of Fig. 6), consequently leading to misclassifications of class labels by the segmentation model employed in calculating mIoU.

Qualitative results. Our approach consistently produces images with heightened sharpness and intricate details. Taking the examples in Fig. 6 (first row), our method notably achieves superior physical coherence between the person and the baseball bat. In contrast, certain GAN-based baselines, such as SPADE, OASIS, and SC-GAN, encounter challenges in synthesizing the person effectively. This might be attributed to inherent limitations in the generative capacity of GANs. While other diffusion-based methods like PITI [38] and FreestyleNet [42] show improved generation of the person, they still grapple with the physical coherence problem due to their inability to capture potential physical coherence restrictions. This observation underscores the ef-

Methods	COCO-stuff			ADE20K		
	FID ↓	mIoU ↑	DS ↑	FID ↓	mIoU ↑	DS ↑
Pix2PixHD[39]	110.7	15.2	-	82.3	20.8	-
SPADE[25]	23.2	36.8	-	33.6	38.2	-
CC-FPSE[19]	20.0	41.5	0.079	32.3	42.5	0.118
OASIS[33]	16.9	43.9	0.328	27.8	48.1	0.282
SC-GAN[41]	17.7	41.8	-	28.4	44.5	-
PITI[38]	15.6	35.8	0.533	27.3	30.6	0.492
FreestyleNet[42]	15.1	41.5	0.591	25.7	42.0	0.587
EOCNet(Ours)	14.2	43.0	0.624	24.6	43.3	0.619

Table 1. Quantitative comparison results with the state-of-the-art LIS methods. Note that Pix2PixHD, SPADE and SC-GAN do not support diverse generations.

fectiveness of our approach in improving physical coherence generation in comparison to existing methods.

4.4. Dual Effectiveness of SCA

Effectiveness on physical coherence generation. Upon meticulous examination of the visualized self-similarity maps of SCA in Fig. 7, a discernible pattern emerges: SCA prominently emphasizes values, particularly in object coherence, such as the joint region of the hand and racket (first sample in Fig. 7). This observation underscores SCA’s effectiveness in enhancing physical coherence within generated images.

Effectiveness on complex texture generation. Furthermore, these visualizations also highlight SCA’s impact on intricate texture generation, evident in emphasized values also within regions with complex texture like facial details, seen in the girl’s face region (second sample in Fig. 7).

We attribute this to the intricate diversity within challenging-to-generate objects like a person’s face and fingers. Achieving effective synthesis in these regions demands models to explore more subtle correlations between pixels. However, existing methods only utilize cross-attention to capture complex correlations, which might be insufficient. This limitation leads to their failure to generate subtle texture variations.

However, our SNF exhibits exceptional sensitivity and adaptability to the diversity and complexity within these regions. This enables our approach to proficiently capture inter-class coherence correlations and intra-class intricate textures, which significantly promotes complex texture generation. We additionally offer qualitative comparisons on complex textures generation with FreestyleNet in Fig. 8.

5. Conclusion

This work addresses the object coherence challenge within the LIS task including semantic coherence and physical coherence. We propose a novel diffusion model with an effective Global Semantic Fusion (GSF) module and a

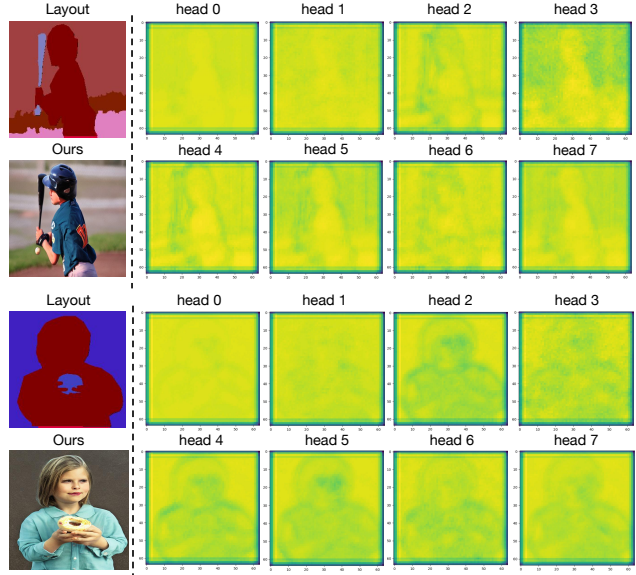


Figure 7. Effectiveness of the proposed SCA. We present visualized average self-similarity maps for each head. Notably, these heatmaps emphasize significant values in the coherence of objects and regions with intricate textures. We omit the grounded text and captions for simplicity.

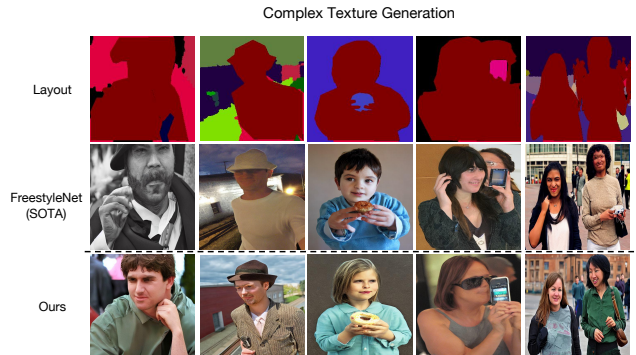


Figure 8. Qualitative comparative results on complex texture generation against the current state-of-the-art model [42]. The captions of all the cases are set to empty for our model and we omit the grounded text for simplicity.

Self-similarity Feature Enhancement (SFE) module. For semantic coherence, we introduce caption as input and develop GSF to fuse the supervision from the layout restriction and semantic coherence requirement and exploit it to guide the image synthesis process. To improve the physical coherence generation, we propose SFE that leverages the effective synergy between Rectified cross-attention (RCA) and Self-similarity Coherence Attention (SCA). It employs SCA to explicitly integrate local contextual physical coherence restriction into each pixel’s generation process while retaining RCA’s superiority in generating previously unseen objects. Comprehensive evaluations showcase superior image quality and enhanced controllability compared to existing methods.

References

- [1] Stephan Alaniz, Thomas Hummel, and Zeynep Akata. Semantic image synthesis with semantically coupled vq-model. *arXiv preprint arXiv:2209.02536*, 2022. 3
- [2] Martin Arjovsky and Léon Bottou. Towards principled methods for training generative adversarial networks. *arXiv preprint arXiv:1701.04862*, 2017. 2
- [3] Fan Bao, Chongxuan Li, Jun Zhu, and Bo Zhang. Analytic-dpm: an analytic estimate of the optimal reverse variance in diffusion probabilistic models. *arXiv preprint arXiv:2201.06503*, 2022. 3
- [4] Holger Caesar, Jasper Uijlings, and Vittorio Ferrari. Cocosuff: Thing and stuff classes in context. In *CVPR*, pages 1209–1218, 2018. 3, 6
- [5] Marlène Careil, Jakob Verbeek, and Stéphane Lathuilière. Few-shot semantic image synthesis with class affinity transfer. In *CVPR*, pages 23611–23620, 2023. 3
- [6] Prafulla Dhariwal and Alexander Nichol. Diffusion models beat gans on image synthesis. In *NeurIPS*, pages 8780–8794, 2021. 3
- [7] Haotian Dong, Enhui Ma, Lubo Wang, Miaohui Wang, Wuyuan Xie, Qing Guo, Ping Li, Lingyu Liang, Kairui Yang, and Di Lin. Cvsformer: Cross-view synthesis transformer for semantic scene completion. *arXiv preprint arXiv:2307.07938*, 2023. 3
- [8] Yutong He, Ruslan Salakhutdinov, and J Zico Kolter. Localized text-to-image generation for free via cross attention control. *arXiv preprint arXiv:2306.14636*, 2023. 2
- [9] Martin Heusel, Hubert Ramsauer, Thomas Unterthiner, Bernhard Nessler, and Sepp Hochreiter. Gans trained by a two time-scale update rule converge to a local nash equilibrium. In *NeurIPS*, 2017. 6
- [10] Jonathan Ho and Tim Salimans. Classifier-free diffusion guidance. *arXiv preprint arXiv:2207.12598*, 2022. 3, 6
- [11] Jonathan Ho, Ajay Jain, and Pieter Abbeel. Denoising diffusion probabilistic models. In *NeurIPS*, pages 6840–6851, 2020. 3
- [12] Phillip Isola, Jun-Yan Zhu, Tinghui Zhou, and Alexei A Efros. Image-to-image translation with conditional adversarial networks. In *CVPR*, pages 1125–1134, 2017. 3
- [13] Chang Jiang, Fei Gao, Biao Ma, Yuhao Lin, Nannan Wang, and Gang Xu. Masked and adaptive transformer for exemplar based image translation. In *CVPR*, pages 22418–22427, 2023. 3
- [14] Bahjat Kawar, Michael Elad, Stefano Ermon, and Jiaming Song. Denoising diffusion restoration models. In *NeurIPS*, pages 23593–23606, 2022. 3
- [15] Nupur Kumari, Bingliang Zhang, Sheng-Yu Wang, Eli Shechtman, Richard Zhang, and Jun-Yan Zhu. Ablating concepts in text-to-image diffusion models. *arXiv preprint arXiv:2303.13516*, 2023. 2, 3
- [16] Junnan Li, Dongxu Li, Silvio Savarese, and Steven Hoi. Blip-2: Bootstrapping language-image pre-training with frozen image encoders and large language models. *arXiv preprint arXiv:2301.12597*, 2023. 6
- [17] Yuheng Li, Haotian Liu, Qingyang Wu, Fangzhou Mu, Jianwei Yang, Jianfeng Gao, Chunyuan Li, and Yong Jae Lee. Gligen: Open-set grounded text-to-image generation. In *CVPR*, pages 22511–22521, 2023. 2
- [18] Luping Liu, Yi Ren, Zhijie Lin, and Zhou Zhao. Pseudo numerical methods for diffusion models on manifolds. *arXiv preprint arXiv:2202.09778*, 2022. 6
- [19] Xihui Liu, Guojun Yin, Jing Shao, Xiaogang Wang, et al. Learning to predict layout-to-image conditional convolutions for semantic image synthesis. In *NeurIPS*, 2019. 2, 3, 6, 8
- [20] Andreas Lugmayr, Martin Danelljan, Andres Romero, Fisher Yu, Radu Timofte, and Luc Van Gool. Repaint: Inpainting using denoising diffusion probabilistic models. In *CVPR*, pages 11461–11471, 2022. 3
- [21] Zhengyao Lv, Xiaoming Li, Xin Li, Fu Li, Tianwei Lin, Dongliang He, and Wangmeng Zuo. Learning semantic person image generation by region-adaptive normalization. In *CVPR*, pages 10806–10815, 2021. 2
- [22] Zhengyao Lv, Xiaoming Li, Zhenxing Niu, Bing Cao, and Wangmeng Zuo. Semantic-shape adaptive feature modulation for semantic image synthesis. In *CVPR*, pages 11214–11223, 2022. 3
- [23] Alexander Quinn Nichol and Prafulla Dhariwal. Improved denoising diffusion probabilistic models. In *ICML*, pages 8162–8171, 2021. 3
- [24] Jihye Park, Sunwoo Kim, Soohyun Kim, Seokju Cho, Jaejun Yoo, Youngjung Uh, and Seungryong Kim. Lanit: Language-driven image-to-image translation for unlabeled data. In *CVPR*, pages 23401–23411, 2023. 3
- [25] Taesung Park, Ming-Yu Liu, Ting-Chun Wang, and Jun-Yan Zhu. Semantic image synthesis with spatially-adaptive normalization. In *CVPR*, pages 2337–2346, 2019. 2, 3, 6, 8
- [26] Alec Radford, Luke Metz, and Soumith Chintala. Unsupervised representation learning with deep convolutional generative adversarial networks. *arXiv preprint arXiv:1511.06434*, 2015. 2
- [27] Alec Radford, Jong Wook Kim, Chris Hallacy, Aditya Ramesh, Gabriel Goh, Sandhini Agarwal, Girish Sastry, Amanda Askell, Pamela Mishkin, Jack Clark, et al. Learning transferable visual models from natural language supervision. In *ICLR*, pages 8748–8763, 2021. 4
- [28] Robin Rombach, Andreas Blattmann, Dominik Lorenz, Patrick Esser, and Björn Ommer. High-resolution image synthesis with latent diffusion models. In *CVPR*, pages 10684–10695, 2022. 2, 3, 6
- [29] Chitwan Saharia, William Chan, Saurabh Saxena, Lala Li, Jay Whang, Emily L Denton, Kamyar Ghasemipour, Raphael Gontijo Lopes, Burcu Karagol Ayan, Tim Salimans, et al. Photorealistic text-to-image diffusion models with deep language understanding. In *NeurIPS*, pages 36479–36494, 2022. 2, 3
- [30] Chitwan Saharia, Jonathan Ho, William Chan, Tim Salimans, David J Fleet, and Mohammad Norouzi. Image super-resolution via iterative refinement. *TPAMI*, 45(4):4713–4726, 2022. 3
- [31] Yupeng Shi, Xiao Liu, Yuxiang Wei, Zhongqin Wu, and Wangmeng Zuo. Retrieval-based spatially adaptive normalization for semantic image synthesis. In *CVPR*, pages 11224–11233, 2022. 3

- [32] Vadim Sushko, Edgar Schönfeld, Dan Zhang, Juergen Gall, Bernt Schiele, and Anna Khoreva. You only need adversarial supervision for semantic image synthesis. *arXiv preprint arXiv:2012.04781*, 2020. [2](#)
- [33] Vadim Sushko, Edgar Schönfeld, Dan Zhang, Juergen Gall, Bernt Schiele, and Anna Khoreva. Oasis: only adversarial supervision for semantic image synthesis. *IJCV*, 130(12): 2903–2923, 2022. [2](#), [3](#), [6](#), [8](#), [11](#)
- [34] Zhentao Tan, Dongdong Chen, Qi Chu, Menglei Chai, Jing Liao, Mingming He, Lu Yuan, Gang Hua, and Nenghai Yu. Efficient semantic image synthesis via class-adaptive normalization. *TPAMI*, 44(9):4852–4866, 2021.
- [35] Zhentao Tan, Qi Chu, Menglei Chai, Dongdong Chen, Jing Liao, Qiankun Liu, Bin Liu, Gang Hua, and Nenghai Yu. Semantic probability distribution modeling for diverse semantic image synthesis. *TPAMI*, 45(5):6247–6264, 2022. [3](#)
- [36] Anwaar Ulhaq, Naveed Akhtar, and Ganna Pogrebna. Efficient diffusion models for vision: A survey. *arXiv preprint arXiv:2210.09292*, 2022. [3](#)
- [37] Ashish Vaswani, Noam Shazeer, Niki Parmar, Jakob Uszkoreit, Llion Jones, Aidan N Gomez, Łukasz Kaiser, and Illia Polosukhin. Attention is all you need. In *NeurIPS*, 2017. [2](#), [4](#)
- [38] Tengfei Wang, Ting Zhang, Bo Zhang, Hao Ouyang, Dong Chen, Qifeng Chen, and Fang Wen. Pretraining is all you need for image-to-image translation. *arXiv preprint arXiv:2205.12952*, 2022. [2](#), [3](#), [6](#), [7](#), [8](#)
- [39] Ting-Chun Wang, Ming-Yu Liu, Jun-Yan Zhu, Andrew Tao, Jan Kautz, and Bryan Catanzaro. High-resolution image synthesis and semantic manipulation with conditional gans. In *CVPR*, pages 8798–8807, 2018. [2](#), [3](#), [6](#), [8](#)
- [40] Weilun Wang, Jianmin Bao, Wengang Zhou, Dongdong Chen, Dong Chen, Lu Yuan, and Houqiang Li. Semantic image synthesis via diffusion models. *arXiv preprint arXiv:2207.00050*, 2022.
- [41] Yi Wang, Lu Qi, Ying-Cong Chen, Xiangyu Zhang, and Jiaya Jia. Image synthesis via semantic composition. In *CVPR*, pages 13749–13758, 2021. [2](#), [3](#), [6](#), [8](#)
- [42] Han Xue, Zhiwu Huang, Qianru Sun, Li Song, and Wenjun Zhang. Freestyle layout-to-image synthesis. In *CVPR*, pages 14256–14266, 2023. [2](#), [3](#), [5](#), [6](#), [7](#), [8](#)
- [43] Ling Yang, Zhilin Huang, Yang Song, Shenda Hong, Guohao Li, Wentao Zhang, Bin Cui, Bernard Ghanem, and Ming-Hsuan Yang. Diffusion-based scene graph to image generation with masked contrastive pre-training. *arXiv preprint arXiv:2211.11138*, 2022. [3](#)
- [44] Guangcong Zheng, Shengming Li, Hui Wang, Taiping Yao, Yang Chen, Shouhong Ding, and Xi Li. Entropy-driven sampling and training scheme for conditional diffusion generation. In *ECCV*, pages 754–769, 2022. [3](#)
- [45] Guangcong Zheng, Xianpan Zhou, Xuewei Li, Zhongang Qi, Ying Shan, and Xi Li. Layoutdiffusion: Controllable diffusion model for layout-to-image generation. In *CVPR*, pages 22490–22499, 2023. [2](#), [5](#)
- [46] Bolei Zhou, Hang Zhao, Xavier Puig, Sanja Fidler, Adela Barriuso, and Antonio Torralba. Scene parsing through ade20k dataset. In *CVPR*, pages 633–641, 2017. [3](#), [6](#)
- [47] Junchen Zhu, Lianli Gao, Jingkuan Song, Yuan-Fang Li, Feng Zheng, Xuelong Li, and Heng Tao Shen. Label-guided generative adversarial network for realistic image synthesis. *TPAMI*, 45(3):3311–3328, 2022. [3](#)
- [48] Peihao Zhu, Rameen Abdal, Yipeng Qin, and Peter Wonka. Sean: Image synthesis with semantic region-adaptive normalization. In *CVPR*, pages 5104–5113, 2020.
- [49] Zhen Zhu, Zhiliang Xu, Ansheng You, and Xiang Bai. Semantically multi-modal image synthesis. In *CVPR*, pages 5467–5476, 2020. [3](#)

A. Supplementary materials

This supplementary material includes the algorithm of Self-similarity Coherence Attention (SCA) in Appendix A.1, the diversity evaluation in Appendix A.2, the supplementary for the effectiveness of SCA in Appendix A.3, the effectiveness of GSF in Appendix A.4, more visual comparisons with LIS baselines in Appendix A.5, limitation discussion in Appendix A.6, and discussions about the societal impact in Appendix A.7.

A.1. Algorithm

The computation pipeline of SCA is illustrated in Algorithm 1.

Algorithm 1 SCA

Input: Input Query \mathcal{Q} , Value V , local context size k

Output: Output image feature O

- 1: Reshape \mathcal{Q} to match $\mathbb{R}^{k^2 \times H \times W}$
 - 2: Get padded feature $F \in \mathbb{R}^{k^2 \times (H+k-1) \times (W+k-1)}$ by adding zero-padding of size $(k-1)/2$ to \mathcal{Q}
 - 3: Initialize an feature map $SS \in \mathbb{R}^{k^2 \times H \times W}$
 - 4: **for** each i in $0, 1, \dots, H-1$ **do**
 - 5: **for** each j in $0, 1, \dots, W-1$ **do**
 - 6: $O \in \mathbb{R}^{C, k^2} \leftarrow$ the flatten features of local $(k \times k)$ region centered at the spatial position (i, j) in F
 - 7: **for** each t in $[0, 1, \dots, k^2]$ **do**
 - 8: $SS_{t, i, j} \leftarrow \sum_{c=0}^C \mathcal{Q}_{c, i, j} * O_{c, t}$.
 - 9: **end for**
 - 10: **end for**
 - 11: **end for**
 - 12: Get the self-similarity maps M by Eq. (9)
 - 13: Get the output image feature maps I_{SCA} by Eq. (10)
-

A.2. Diversity evaluation

Our model naturally facilitates diverse image generation from a single layout using different texts and captions (refer to Fig. 1 and Fig. 5 in the main paper). We assess diversity akin to OASIS [33]. Specifically, the Diversity Score (DS) is computed between images generated from identical layouts (and the same text for our model) with randomly sampled noise. Evaluation results are detailed in Tab. 1 in the main paper, where our model achieves the highest DS compared to all other methods. Here, we provide some visual examples of our model in Fig. 11.

A.3. More visualized self-similarity maps

We provide more visualized self-similarity maps in Fig. 12.

A.4. Effectiveness of GSF

GSF fuses supervision information from the layout restriction and caption requirement and infuses amalgamated su-

pervision features into the noise image to steer the image synthesis effectively, thereby enhancing semantic coherence control over image generation.

To evaluate the effectiveness of GSF, we conduct ablation experiments by directly removing GSF. Notably, in its absence, we observed the stylistic inconsistency problem within generated images as shown in Fig. 13. Certain objects exhibited styles that deviated from the overall scene, leading to unsatisfied image generation. This observation demonstrated GSF’s additional effectiveness in maintaining the style consistency of generated images.

Further, we experiment with a naive approach to control semantic coherence in generated images. This involved concatenating the caption and grounded text, allowing the semantic information to interact with noisy images within cross-attention layers. The qualitative results are depicted in 14. It is evident that this method is ineffective as it addresses the highly relevant layout restriction and semantic coherence requirement separately while the relative positions of objects in the layout would inevitably influence their semantic coherence interactions.

These experimental results undoubtedly demonstrated the indispensable role of GSF in elevating both the controllability and synthesis quality, aligning with the primary goals of our research.

A.5. More qualitative comparisons with LIS baselines

We provide more qualitative comparative results against the LIS baselines on COCO-stuff and ADE20K in Fig. 15 and Fig. 16 respectively.

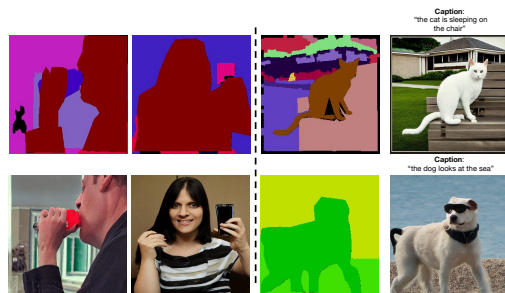


Figure 9. Failure cases.

A.6. Limitations

Several failure cases of our method are illustrated in Fig. 9. Our approach showcases enhanced capabilities in most object coherence and complex texture generation. However, we fail to generate certain scenarios well, such as generating extremely intricate textures resembling hands (Fig. 9 (left)). Moreover, despite the integration of caption-guided semantic coherence control in our method, our model struggles to

achieve semantic alignment when conflicts arise between the semantic coherence requirement specified in the caption and the underlying layout (Fig. 9 (right)). These limitations underscore the need for further exploration.

A.7. Societal impact

Our work has a multifaceted societal impact, offering opportunities for creative expression and responsible application. Our method facilitates diverse image generation via layout, text, and caption manipulation, which unleashes users' power to enhance their creativity for more personalized image creation. This innovation opens new horizons in content creation and artistic exploration, with potentially transformative effects on industries like entertainment, advertising, and design that seek tailored and contextually rich visuals.

Physical Coherence



Figure 10. We present more cases of prevailing challenges of the physical coherence problem. We omit the grounded text for simplicity.

Layout

Diverse Generation

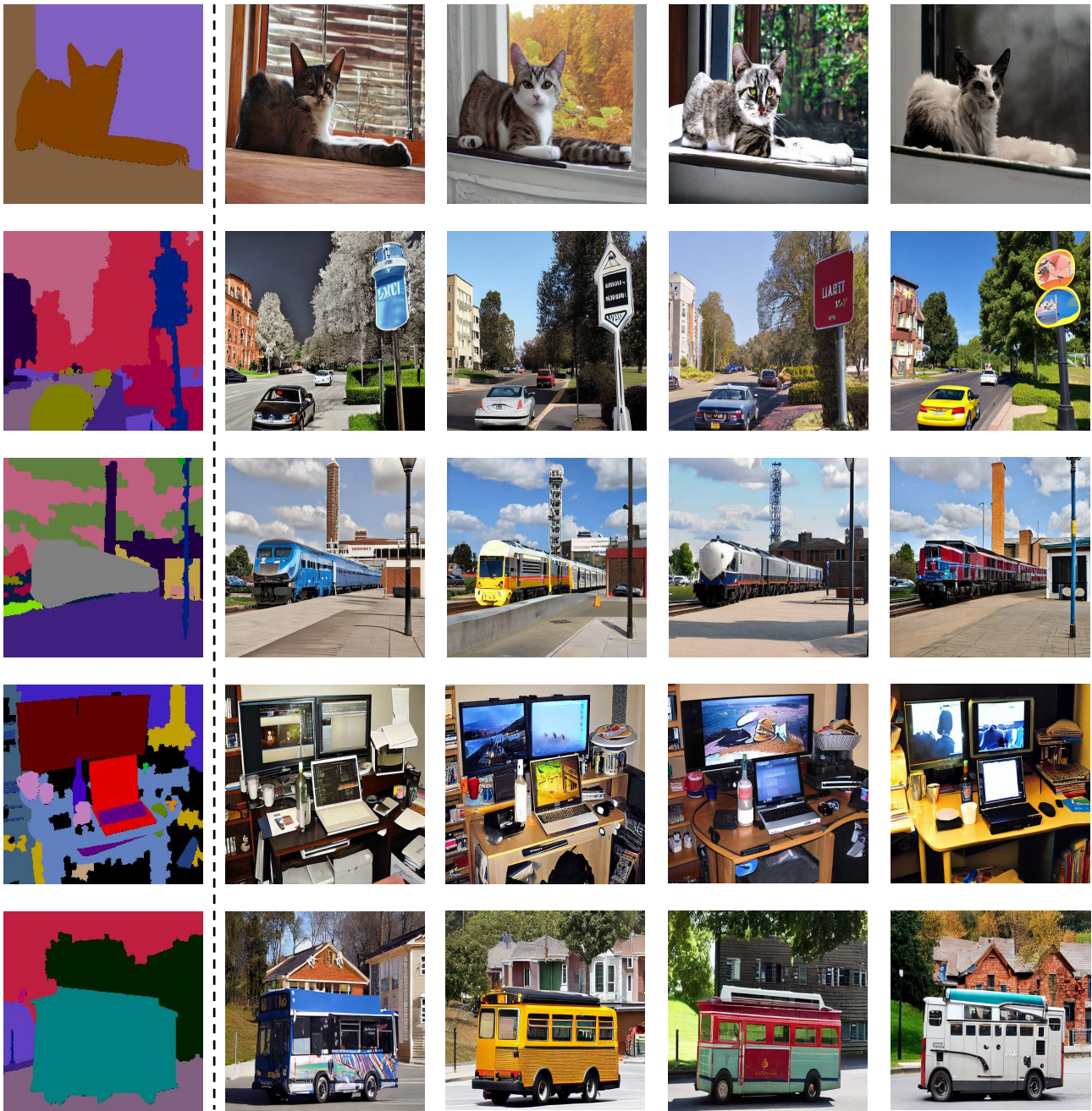


Figure 11. Diverse generation results of our proposed model. The captions in these cases are set to empty and we omit the grounded text for simplicity.

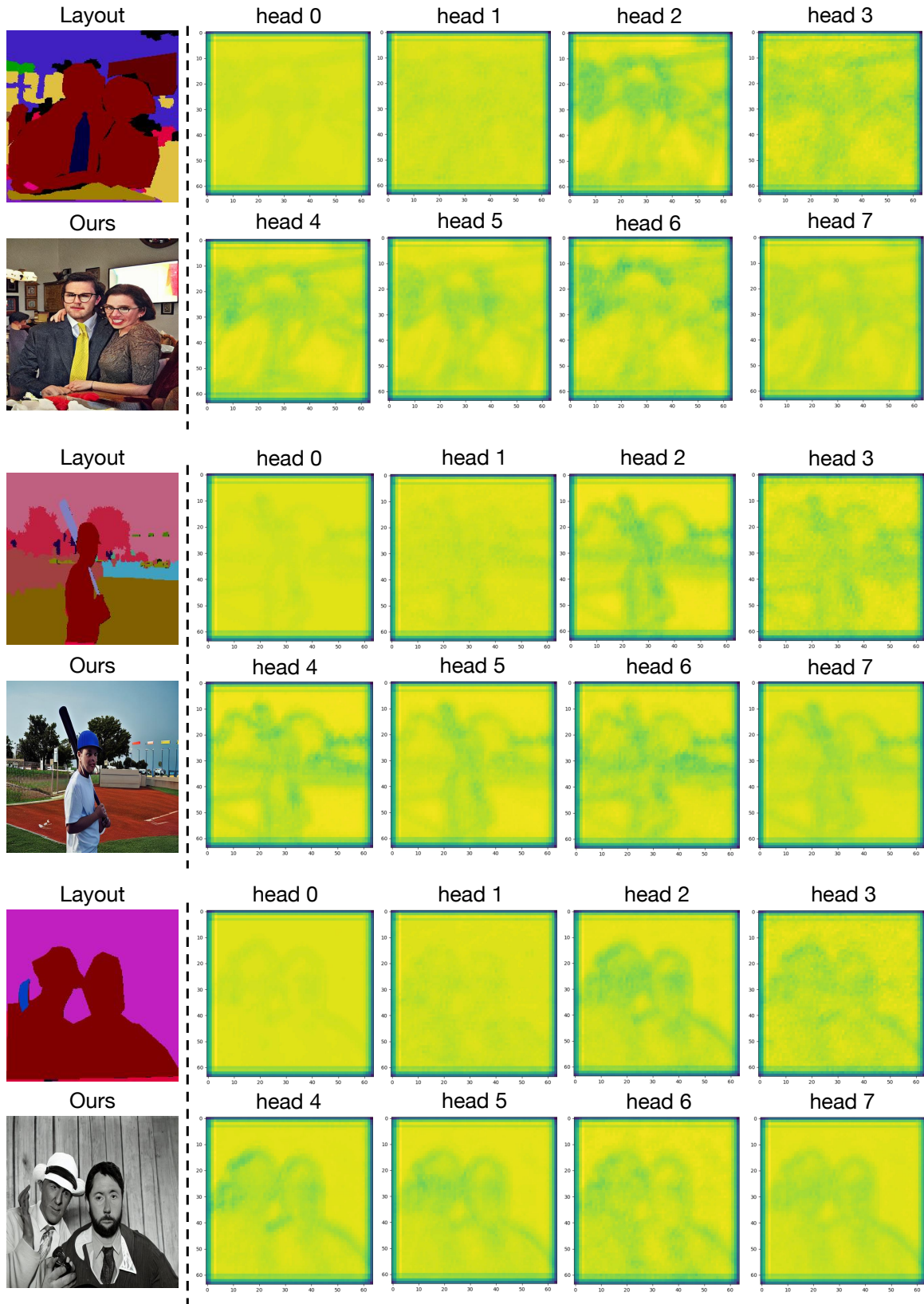


Figure 12. We present more visualized self-similarity maps. The captions in these cases are set to empty and we omit the grounded text for simplicity.

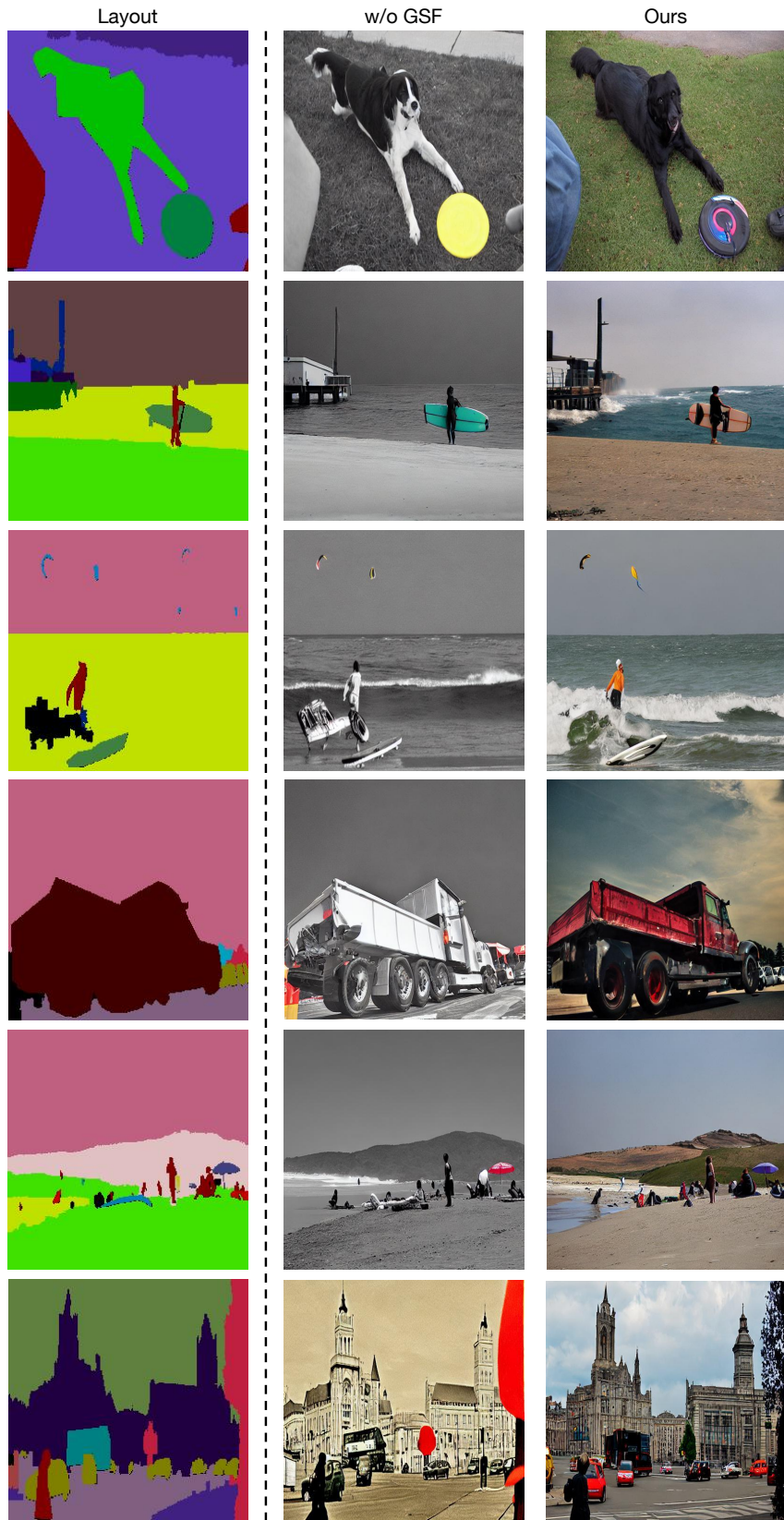


Figure 13. Effectiveness of the proposed GSF. The removal of GSF results in stylistic inconsistency among the generated images. The captions in these cases are set to empty and we omit the grounded text for simplicity.

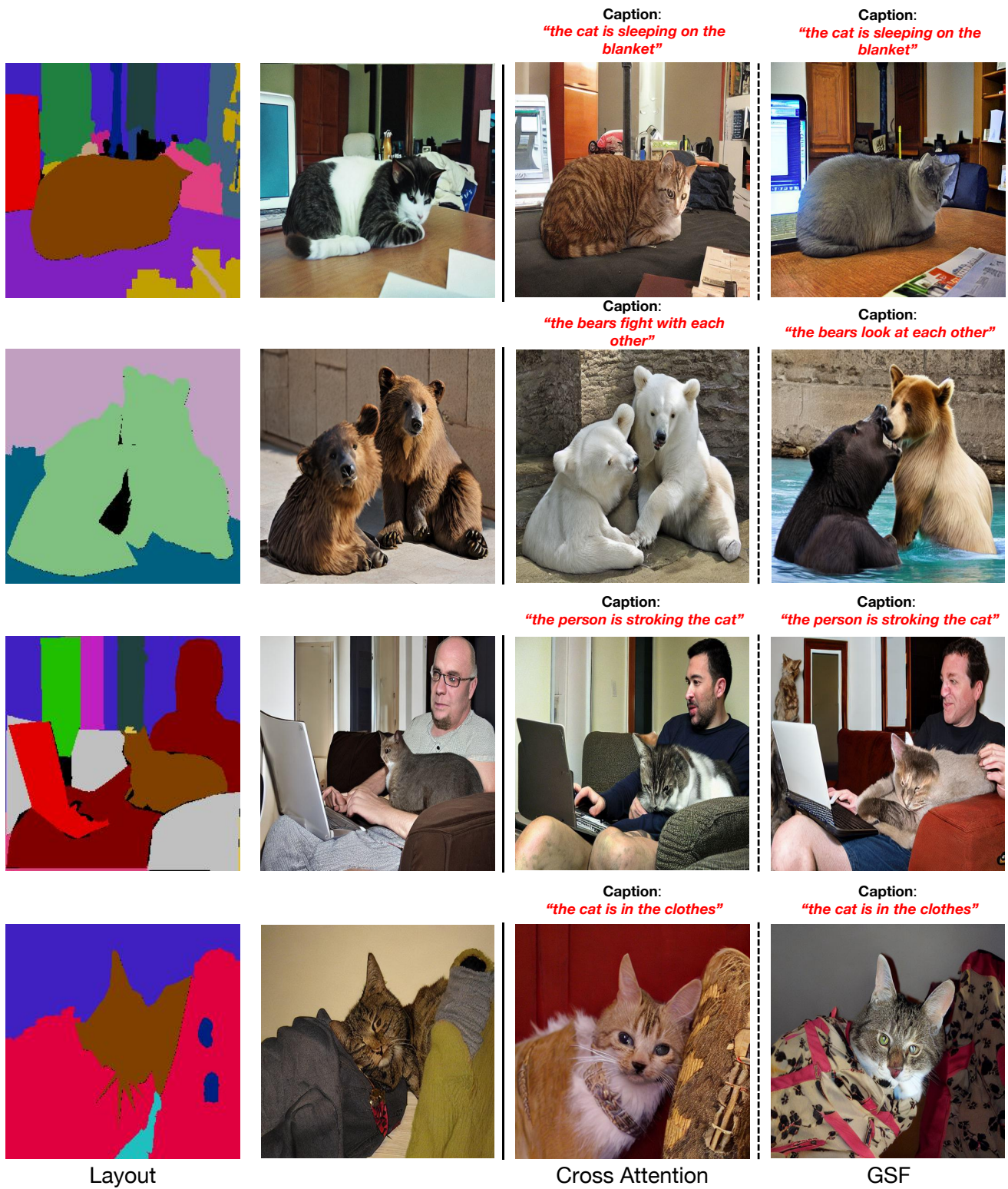


Figure 14. Qualitative results against the method of directly concatenating the caption and grounded text to integrate semantic information into the generation process. We omit the grounded text for simplicity.

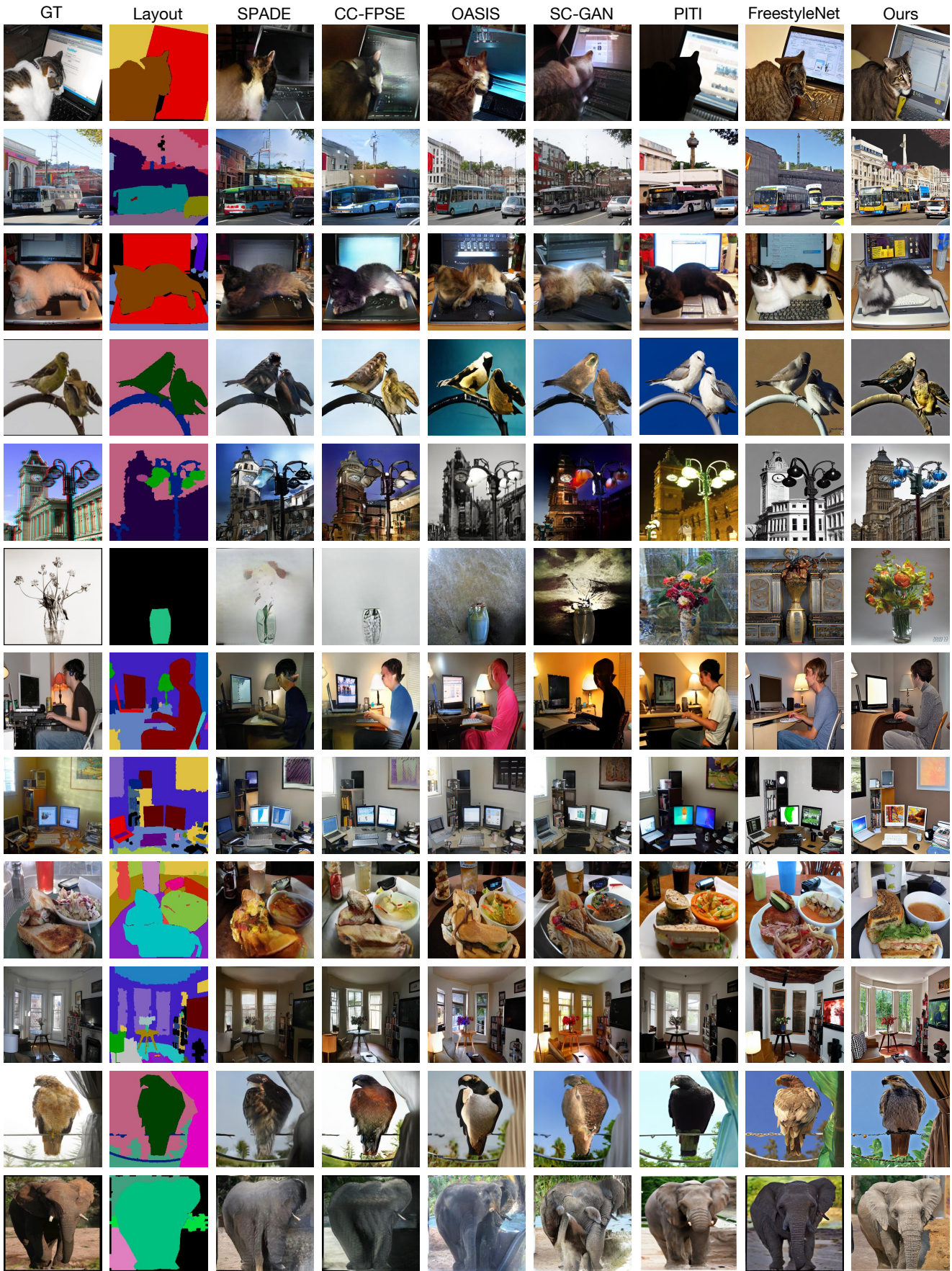


Figure 15. More qualitative comparison results with LIS baselines on COCO-stuff. The captions of our model in these cases are set to empty and we omit the grounded text for simplicity.

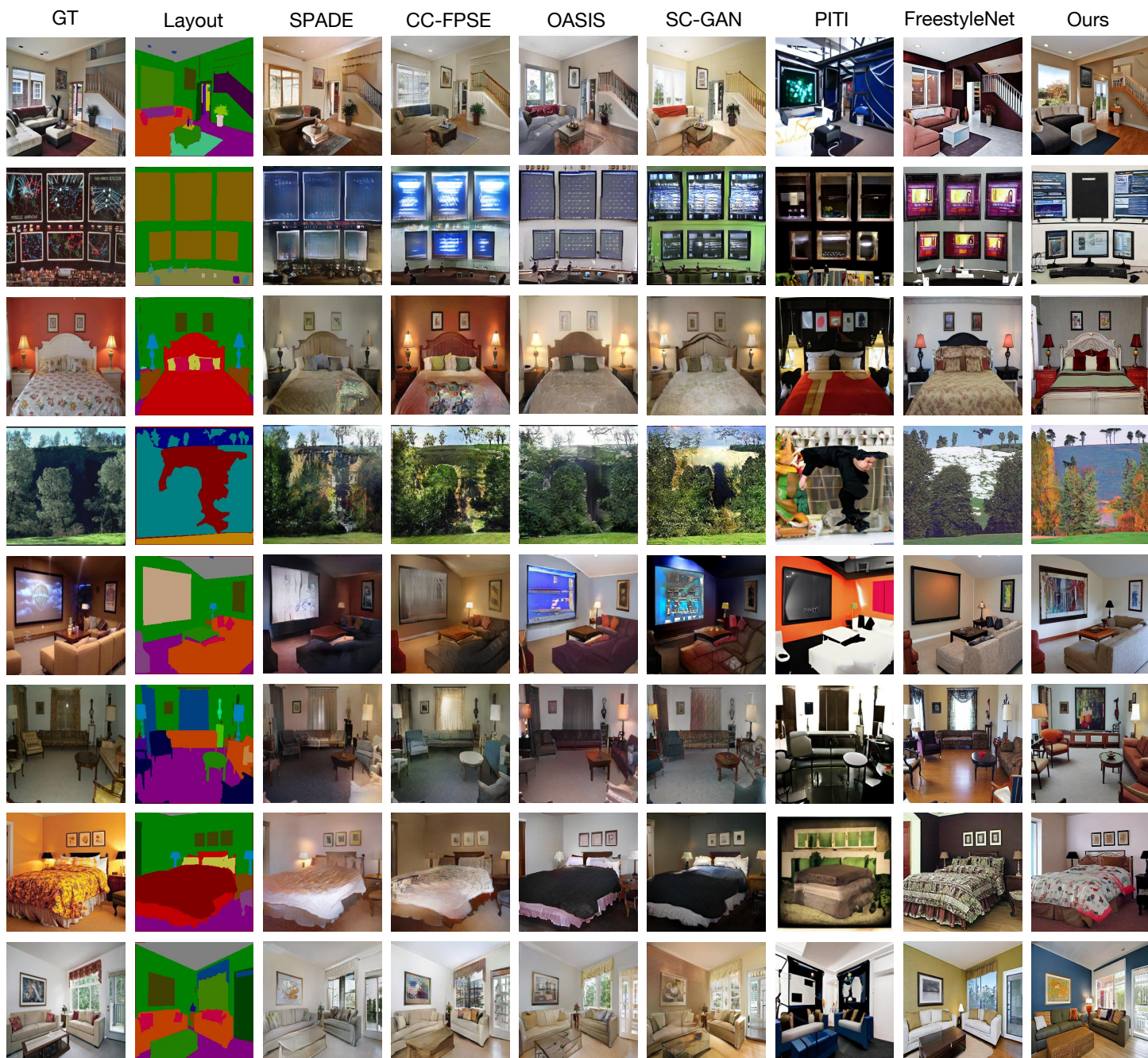


Figure 16. More qualitative comparison results with LIS baselines on ADE20K. The captions of our model in these cases are set to empty and we omit the grounded text for simplicity.